Journal of Structural Biology 194 (2016) 90–101

Contents lists available at ScienceDirect

Journal of Structural Biology

journal homepage: www.elsevier.com/locate/yjsbi

Helicobacter pylori cell binding factor 2: Insights into domain motion

Vankadari Naveen [a,b,1], Chen-Hsi Chu [c,1], Bo-Wei Chen [c], Yen-Chun Tsai [c], Chwan-Deng Hsiao [a,b,*], Yuh-Ju Sun [c,*]

[a] Molecular Cell Biology, Taiwan International Graduate Program, Graduate Institute of Life Sciences, National Defense Medical Center and Academia Sinica, Taipei 115, Taiwan
[b] Institute of Molecular Biology, Academia Sinica, Taipei 115, Taiwan
[c] Institute of Bioinformatics and Structural Biology, National Tsing Hua University, Hsinchu 300, Taiwan

ARTICLE INFO

Article history:
Received 18 September 2015
Received in revised form 22 December 2015
Accepted 2 February 2016
Available online 2 February 2016

Keywords:
Cell-binding factor 2
Chaperone
Domain motion
Helicobacter pylori
PPIase

ABSTRACT

Helicobacter pylori cell binding factor 2 (*Hp*CBF2) is an antigenic virulence factor belonging to the SurA-like peptidyl-prolyl *cis–trans* isomerase family with implications for pathogenicity in the human gastrointestinal tract. *Hp*CBF2 possesses PPIase activity and could act as a periplasmic chaperone to regulate outer membrane protein assembly. Here, we measured the isomerization and chaperone activity of *Hp*CBF2, and determined the crystal structure of *Hp*CBF2 in complex with an inhibitor, indole-2-carboxylic acid (I2CA), at 2.4 Å resolution. *Hp*CBF2-I2CA forms a homodimer encasing a large central hydrophobic cavity with a basket-like structure, and each monomer contains a PPIase and a chaperone domain. In the *Hp*CBF2-I2CA dimer, the two PPIase domains separate by a distance of 22.8 Å, while the two chaperone domains arrange in a domain-swap manner. The PPIase domains bound with I2CA ligand face towards the chaperone domains and are shielded by surrounding hydrophobic residues. With the aid of SAXS experiments, we also revealed domain motion between the apo- and I2CA-bound states of *Hp*CBF2. The domain motion in *Hp*CBF2 might be necessary for the isomerization activity of PPIase and the accommodation of the unfolded and partially folded peptides to refold by chaperone domain.

© 2016 Elsevier Inc. All rights reserved.

1. Introduction

All amino acid residues energetically favor the *trans* rather than the *cis* conformation, except for proline which can adopt distinct *trans* or *cis* conformations between Xxx-Pro motifs (where Xxx could be any residue) (Pierson et al., 2013). Peptidyl-prolyl *cis–trans* isomerase (PPIase) catalyzes prolyl *cis–trans* isomerization to alter the conformation of proteins. Prolyl *cis–trans* isomerization acts as a molecular timer in the cell cycle, cell signaling, gene expression, immune responses, neuronal function, and infection (Lu et al., 2007). Cyclophilins (Lang et al., 1987), FK506-binding proteins (FKBP) (Siekierka et al., 1989), and parvulins (Rahfeld et al., 1994) are three typical families of PPIase. Among the parvulin family, human Pin1 (*Hs*Pin1) is the most well-characterized eukaryotic PPIase and is unique in recognizing phosphorylated Ser/Thr-Pro motifs (Liou et al., 2011). Pin1 is involved in several important cellular processes, including cell-cycle progression, neuronal function, cancer progression and immune responses, etc. (Girardini et al., 2011; Lee et al., 2011; Lu and Zhou, 2007). However, Pin1 lacks a distinct chaperone domain, as found in prokaryotic PPIases, and also differs from other PPIases in its substrate specificity for phosphorylated peptide substrate (Liou et al., 2011). Juglone (5-hydroxy-1,4-naphthoquinone) (Hennig et al., 1998) and I2CA (indole 2-carboxylic acid) (Potter et al., 2010) are two well-characterized inhibitors of parvulin-type PPIase. In prokaryotes, *Escherichia coli* SurA (*Ec*SurA) is the best studied parvulin-type PPIase, functioning as a molecular chaperone that facilitates correct folding of outer membrane proteins (Lazar and Kolter, 1996). Unlike other proteins, *Ec*SurA consists of two parvulin-type PPIase domains and one chaperone domain encompassing the *N*- and *C*-terminal regions of the protein (Bitto and McKay, 2002). Recently, numerous SurA-like PPIase have been reported that contain one parvulin-type PPIase domain and one chaperone domain, e.g. *Bordetella pertussis* Par27 (Clantin et al., 2010), *Leptospira interrogans* LIC12922 (Giuseppe et al., 2011), *Campylobacter jejuni* PEB4 (*Cj*PEB4) (Kale et al., 2011), and *Bacillus subtilis* PrsA (*Bs*PrsA) (Jakob et al., 2015).

*Abbreviations: Hp*CBF2, *Helicobacter pylori* cell-binding factor 2; I2CA, indole-2-carboxylic acid.

* Corresponding authors at: Institute of Molecular Biology, Academia Sinica, Taipei 115, Taiwan, ROC (C.-D. Hsiao). Institute of Bioinformatics and Structural Biology, National Tsing Hua University, Hsinchu 300, Taiwan, ROC (Y.-J. Sun).
E-mail addresses: hsiao@gate.sinica.edu.tw (C.-D. Hsiao), yjsun@life.nthu.edu.tw (Y.-J. Sun).
[1] These authors contributed equally to this work.

http://dx.doi.org/10.1016/j.jsb.2016.02.002
1047-8477/© 2016 Elsevier Inc. All rights reserved.

The secreted PPIase of *Helicobacter pylori*, termed *Hp*CBF2 (in this study) or HP0175, is characterized by its *C*-terminal peptidyl-prolyl *cis–trans* isomerase core that has been identified through sequence homology matching (Marchler-Bauer et al., 2015) (www.ncbi.org.gov). *Hp*CBF2 is one of the highly and consistently reactive antigens recognized in human sera (Atanassov et al., 2002; McAtee et al., 1998), acting as a virulence factor and identified as a potential marker for gastric disease-associated *H. pylori* (Gong et al., 2011). *Hp*CBF2 interacts with TLR4 and induces apoptosis of gastric epithelial cells (Basak et al., 2005). *Hp*CBF2 activates NF-kB-driven *IL-6* gene transcription and stimulates release of IL-6 from human macrophages (Pathak et al., 2006). In patients with *H. pylori* infection and distal gastric adenocarcinoma, *Hp*CBF2 transactivates EGFR and drives Th17 inflammation (Amedei et al., 2014; Basu et al., 2008). *Hp*CBF2 is also related to UPR-dependent autophagy and apoptosis in *H. pylori* pathogenesis (Halder et al., 2015). As *Hp*CBF2 possesses several key biological functions, it could be considered a potential target for novel antimicrobial drugs.

*Hp*CBF2 contains a parvulin-type PPIase domain (residues 157–253) for peptidyl-prolyl *cis–trans* isomerization and a chaperone domain for prevention of protein aggregation comprising the *N*-terminal (residues 1–147) and *C*-terminal (residues 262–299) regions. *Cj*PEB4, a homolog of *Hp*CBF2 protein, contains a similar class of PPIase domain and a chaperone domain and the three-dimensional structure of its apo form has been determined (Kale et al., 2011). However, information regarding structural conformation dynamics upon binding to ligands, substrates or inhibitors is lacking for the prokaryotic parvulin-type PPIase. Despite the biological importance of *Hp*CBF2 in gastric cancer and disease, its 3D structure in apo- or ligand-bound state remains unclear. In addition, structural and functional coordination studies of the PPIase and chaperone domain of the SurA-like parvulin PPIase have yet to be undertaken.

Here, we measured the isomerization activity and chaperone activity of *Hp*CBF2, and solved the crystal structure of *Hp*CBF2 in complex with inhibitor I2CA (*Hp*CBF2-I2CA). Meanwhile, we also performed the solution scattering experiments to demonstrate the domain motion of the apo- and I2CA-bound *Hp*CBF2 in solution.

2. Materials and methods

2.1. Cloning, expression, and protein purification

The *Hp0175* gene encoding *Hp*CBF2, but excluding the signal sequence (*N*-terminal residues 1–32), was PCR amplified using the forward primer 5′-CATGCCATGGGCAACACGAAAAAAACGACT GATTC-3′ and the reverse primer 5′-TAACTCGAGCTTGTTGATA CAATTTTAGCGTGC-3′ and cloned into the pET28a vector (Novagen) to produce the *Hp*CBF2 protein with a $(His)_6$-tag at the C terminus. *E. coli* BL21 (DE3) strain transformed with the constructed plasmid was grown and induced by isopropyl-β-D-thiogalactopyranoside (IPTG) in Luria–Bertani (LB) broth with kanamycin (25 μg/ml) at 37 °C. All purification procedures were performed at 4 °C. Cell pellets were pooled and suspended in 10 ml of 20 mM Tris–HCl (pH 7.8), 500 mM NaCl and 10 mM Imidazole (buffer A) per gram of cell paste. The cell suspension was passed through a high-pressure homogenizer (EmulsiFlex-C3), and then centrifuged at 14,000 rpm for 20 min. The supernatant was loaded onto a HisTrap HP (Ni–NTA) column (GE Healthcare) equilibrated with buffer A. The bound *Hp*CBF2 was step-eluted with 10, 30, 300 and 1000 mM imidazole concentrations in buffer A (Supplemental Fig. S1). Eluted fractions were further subjected to analytical ultracentrifugation to elucidate the molar mass of the purified protein. Sedimentation occurred at ~61 kDa, suggesting the presence of stable dimer (Supplemental Fig. S2). Selenomethionine (SeMet)-derivative *Hp*CBF2 protein was produced using T7 Express© (New England Biolabs) cells, and grown in 1 L Le-Master media containing SeMet supplemented with 25 μg ml^{-1} kanamycin. Purification of SeMet-*Hp*CBF2 protein was performed as described for native *Hp*CBF2 above.

2.2. PPIase activity of HpCBF2

The *cis–trans* isomerization activity of *Hp*CBF2 (residues 33–299) was measured by a coupled assay with chymotrypsin, which cleaves the peptide only when the Ala-Pro substrate is in the *trans* state (Giuseppe et al., 2011; Ikolo et al., 2015; Tatara et al., 2009). The oligo peptide, *N*-succinyl-Ala-Ala-Pro-Phe-*p*-nitroanilide (Sigma–Aldrich, Suc-AAPF-*p*NA), was dissolved in tetrahydrofuran (THF) containing 470 mM lithium chloride ($LiCl_2$). The reaction was carried out in 100 mM sodium phosphate (pH 7.8) with 10 μM α-chymotrypsin (Sigma–Aldrich) dissolved in 1 mM HCl at 15 °C. The 50 nM *Hp*CBF2 was tested against varying concentrations (30, 40, and 50 μM) of Suc-AAPF-*p*NA with four independent replicates. Absorbance of chromogenic *p*-nitroaniline at 390 nm was monitored for 3 min in a Hitachi U-3310 UV–Vis Spectrophotometer at 15 °C. The first-order rate constant of released *p*-nitroanilide in the presence or absence of *Hp*CBF2 was calculated by the equation $(k = -\ln[(A_\infty - A_t)/(A_\infty - A_0)]/t)$, where A_∞ is the final absorbance of chromogenic product, A_t is the absorbance at time t, and A_0 is the amplitude of the first phase of isomer-specific proteolysis (Kullertz et al., 1998). The k_{cat}/K_m values were calculated according to the equation $k_{cat}/K_m = (k_{obs} - k_0)/[\text{PPIase}]$ (Motohashi et al., 2003), where k_0 is the first-order rate constant for spontaneous *cis–trans* peptide bond isomerization.

2.3. Chaperone activity of HpCBF2

Chaperone activity of *Hp*CBF2 was assessed by the rate decreased aggregation of chemically-denatured lysozyme (Sigma-Aldrich) as described (Hodak et al., 2008). Fifteen micromolar of lysozyme was first denatured for 2 h at 25 °C in 50 mM Tris–HCl, pH 8.0, containing 6 M guanidine–HCl, 250 mM NaCl and 50 mM DTT, and the rate of aggregation was monitored in the presence of varying *Hp*CBF2 concentrations (7.5 μM, 15 μM and 30 μM) for 600 s. The aggregation rate in the presence of *Hp*CBF2 was measured at UV absorbance 320 nm. As a negative control, 15 μM of BSA (Sigma) was added to the denatured lysozyme and similarly monitored (data not shown).

2.4. Crystallization

For the preparation of native and SeMet-derived *Hp*CBF2-I2CA complex, both proteins (25–30 mg/ml, in 20 mM Tris–HCl, pH 7.8) were incubated with I2CA (Sigma-Aldrich) in a molar ratio of 1:4 at 4 °C for 1 h. Initial crystallization conditions were obtained using Hampton Research crystal screen kits and then optimized to obtain diffraction-quality crystals. The native and SeMet-derived *Hp*CBF2-I2CA complex crystals were crystallized in ~44% (v/v) Jeffamine-M600 (pH 7.0) (Hampton Research) and 50 mM succinate pH 3.5 at 10 °C by the hanging-drop vapor-diffusion method. *Hp*CBF2-I2CA complex crystals were measured as 0.3 × 0.1 × 0.1 mm.

2.5. Data collection, structural determination, and refinement

*Hp*CBF2-I2CA complex crystals were flash frozen in liquid nitrogen and kept under a stream of cold nitrogen (100 K) during data collection using the synchrotron radiation X-ray source

at the National Synchrotron Radiation Research Center (Taiwan) beam line BL13B1. Initial phase determination trials for native diffraction of the *Hp*CBF2-I2CA complex were attempted using available models of *Ec*SurA (PDB ID: 1M5Y) without the P1 domain and *Cj*PEB4 (PDB ID: 3RFW) through Molecular Replacement (MR). However, it was unsuccessful and might be due to orientation or conformational differences between the PPIase and chaperone domains in the *Hp*CBF2-I2CA complex compared to those of apo-*Ec*SurA and apo-*Cj*PEB4. Hence, for the phase determination, anomalous data from SeMet-*Hp*CBF2-I2CA crystals were collected at 3.1 Å resolution on the BL13B1 beamline at the National Synchrotron Radiation Research Center (Hsinchu, Taiwan), and the data was processed using the *HKL*-2000 (Otwinowski and Minor, 1997). SeMet-*Hp*CBF2-I2CA crystals belong to space group $P3_121$, with unit cell dimensions of a = b = 61.7 Å and c = 367.3 Å. The V_M (Matthews, 1968) was calculated as 3.16 $Å^3$ Da^{-1}, which corresponds to a solvent content of 61% for two molecules per asymmetric unit. The structural phase of SeMet-*Hp*CBF2-I2CA was obtained by selenomethionine SAD. AutoSol (Terwilliger et al., 2009) was used to identify selenium sites, the electron density map calculation, and to build the preliminary structural model. Model building was done using *Coot* (Emsley and Cowtan, 2004), and refinement was done using PHENIX (Adams et al., 2010). Non-crystallographic symmetry (NCS) restraints were applied for restrained refinement. The geometric quality of the structures was assessed using Ramachandran plots generated by *MolProbity* (Adams et al., 2010; Davis et al., 2007). Data collection and refinement statistics were summarized in Table 1. PyMoL was used to generate the figures (Delano, 2010).

2.6. Small-angle X-ray scattering (SAXS)

SAXS measurements were performed at the National Synchrotron Radiation Research Center, Taiwan on a BL23A beamline, equipped with a MAR 165 CCD area detector at a sample-to-detector distance of 2.5 m. The protein sample concentration was 25 mg/ml for both apo- and I2CA-bound *Hp*CBF2. The buffer for gel filtration, 20 mM Tris–HCl (pH 7.8)/50 mM Succinate (pH 3.5) (1:1, V/V), with (for I2CA-bound *Hp*CBF2) or without I2CA (for apo *Hp*CBF2), was used as the solvent blank. The X-ray energy was 14.0 keV and the collection time was 300 s. No sample aggregation was observed during the measurements. Background scattering from the buffer alone was subtracted from the sample and the data was scaled using PRIMUS (Konarev et al., 2003). Primary data reduction was performed using an in-house program, and the processed data were analyzed using the ATSAS package software (Petoukhov et al., 2007). The radius of gyration (R_g) was calculated from a Guinier plot using PRIMUS (Konarev et al., 2003). The pair distance distribution function $P(r)$ and the maximum intramolecular distance D_{max} were calculated using GNOM (Svergun, 1992). Shape reconstructions were done with the program DAMMIN (Svergun, 1999). The dummy atom models resulting from 20 individual DAMMIN runs were aligned, averaged, and scored with a normalized spatial discrepancy (NSD) using the program package DAMAVER (Konarev et al., 2003). Models with a large NSD were rejected. The resulting probability models were filtered to a most probable model using DAMFILT (Volkov and Svergun, 2003). The SAXS envelopes of apo- and I2CA-bound *Hp*CBF2 were superimposed with the *Hp*CBF2-I2CA structure using SUPCOMB (Kozin and Svergun, 2001). The *Hp*CBF2-I2CA complex structure (PDB ID: 5EZ1, in this study) was fitted with the filtered models using FoXS program (Schneidman-Duhovny et al., 2010, 2013). Data collection and other SAXS measurements, together with the programs used, are summarized in Table S1.

Table 1
X-ray data collection and refinement statistics of *Hp*CBF2-I2CA complex.

	Native	Se-Met
Data collection statistics		
Source	NSRRC 13B1	NSRRC 13B1
Wavelength (Å)	1.000	0.9763
Space group	$P3_121$	$P3_121$
Resolution (Å)	30.0–2.40 (2.49–2.40)[a]	3.1
Unit cell parameters		
a, *b*, *c* (Å)	*a* = *b* = 62.0, *c* = 366.4	*a* = *b* = 61.7, *c* = 367.3
No. of reflections	187,808	335,083
No. of unique reflections	33,151 (3,054)[a]	15,742
Multiplicity	5.7 (3.0)[a]	21.3
Completeness (%)	98.9 (92.8)[a]	99.9 (100.0)[a]
I/σ (I)	30.2 (1.6)[a]	74.9 (15.8)[a]
R_{merge}[b] (%)	4.5 (50.7)[a]	8.8 (45.2)[a]
$CC_{1/2}$	0.999 (0.753)[a]	
Refinement statistics		
Resolution (Å)	30.0–2.40	
R_{work}[c]/R_{free}[d] (%)	24.4/30.0	
No. of reflections in working set	29,902	
No. of reflections in test set	1,530	
No. of protomers in asymmetric unit	2	
No. of residues	463	
No. of protein atoms	3,760	
No. of water molecules	151	
Ligand (I2CA)	2	
R.m.s.d. bonds length (Å)	0.01	
R.m.s.d. bonds angles (°)	1.25	
Average *B* factors (Å^2)		
All protein atoms	61.6	
I2CA	91.6	
Water	41.4	
Overall	64.9	
MolProbity validation		
Ramachandran plot (%)		
Favored	98.9	
Allowed	1.1	

[a] Values in parentheses are for the highest-resolution shell.
[b] $R_{merge} = \Sigma_{hkl}\Sigma_i|I_i(hkl) - \langle I(hkl)\rangle|/\Sigma_{hkl}\Sigma_i I_i(hkl)$, where $\langle I(hkl)\rangle$ is the mean of the several individual measurements $I_i(hkl)$ of the intensity of reflection *hkl*.
[c] $R_{work} = \Sigma_{hkl}||F_{obs}| - |F_{calc}||/\Sigma_{hkl}|F_{obs}|$, where F_{obs} and F_{calc} are the observed and calculated structure factor amplitudes, respectively.
[d] R_{free} was calculated with 5% of the total number of reflections randomly omitted from the refinement.

2.7. Accession number

The atomic coordinates for the *Hp*CBF2-I2CA complex have been deposited in the RCSB Protein Data Bank under the accession code 5EZ1.

3. Results and discussion

3.1. Multiple sequence alignment of SurA-like PPIase proteins

The *Hp*CBF2 full-length protein sequence was analyzed by Conserved Domain Database (CDD) (Marchler-Bauer et al., 2015) and the results showed that residues 26–299 and 71–298 of *Hp*CBF2 belong to the SurA family (parvulin-like peptidyl-prolyl isomerase) and PrsA family (peptidylprolyl isomerase), respectively. Multiple sequence alignment of *Hp*CBF2 with four parvulin-type PPIase proteins, *Cj*PEB4 (PDB ID: 3RFW) (Kale et al., 2011), *Bs*PrsA (PDB ID: 4WO7) (Jakob et al., 2015), *Ec*SurA (PDB ID: 1MY5, without the non-functional PPIase P1 domain) (Bitto and McKay, 2002), and *Homo sapiens* PIN1 (PDB ID: 1PIN) (Ranganathan et al., 1997) is shown in Fig. 1. *Hp*CBF2 shares 22–35% sequence identity with these four proteins, and the PPIase domain was found to be highly

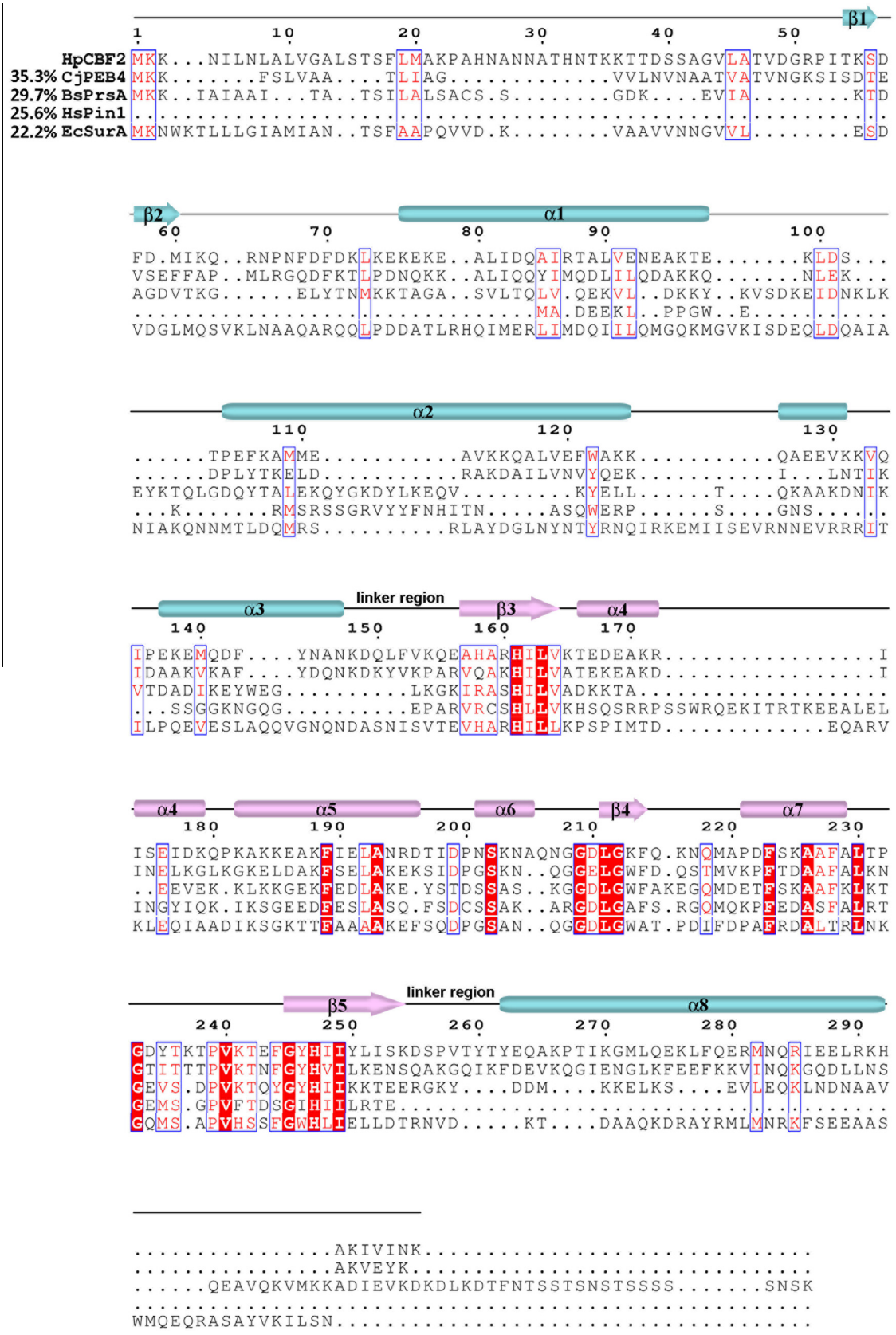

Fig. 1. Multiple sequence alignment of parvulin-type PPIase family proteins. Sequence alignment of *Hp*CBF2 with *Campylobacter jejuni* PEB4 (*Cj*PEB4), *Bacillus subtilis* PrsA (*Bs*PrsA), *Homo sapiens* PIN1 (*Hs*PIN1), and *Escherichia coli* SurA (*Ec*SurA, without its non-functional PPIase P1 domain) generated with ESPript (Gouet et al., 1999). Fully conserved residues are shaded in red, and regions with similar residues are boxed in blue. The secondary structure of *Hp*CBF2 is shown above the sequence alignment. The α-helices are indicated by cylinders and β-strands are indicated by arrows. The PPIase and chaperone domains are colored as pink and cyan, respectively.

conserved. Residues 151–260 of *Hp*CBF2 represent the PPIase domain, which aligns well to the protein sequences of *Cj*PEB4, *Bs*PrsA and *Ec*SurA. In contrast, the *N*- and *C*-terminal residues containing the chaperone domains of *Hp*CBF2 (residues 1–150 and 261–299), *Cj*PEB4, *Bs*PrsA and *Ec*SurA were relatively non-conserved.

3.2. Isomerization activity

The isomerization activity of *Hp*CBF2 was measured in a coupled assay with chymotrypsin, employing the synthetic peptide Suc-AAPF-*p*NA as substrate as described earlier (Bose and Freedman, 1994; Ikolo et al., 2015). As shown in Fig. 2, increased concentrations of Suc-AAPF-*p*NA resulted in increased absorbance at 390 nm, indicating enhanced catalysis by *Hp*CBF2 and increased the amount of free *p*-nitroanilide chromogen. A twofold increase in intensity was observed in the presence of *Hp*CBF2 compared to control without the enzyme. The k_{cat}/K_m for 50 nM *Hp*CBF2 was measured at $236 \pm 7.2\ mM^{-1}\ s^{-1}$, $284 \pm 7.2\ mM^{-1}\ s^{-1}$ and $328 \pm 7.2\ mM^{-1}\ s^{-1}$ for concentrations of 30, 40 and 50 μM of Suc-AAPF-*p*NA, respectively for the four replicates (Fig. 2), demonstrating that the recombinant *Hp*CBF2 possesses isomerization activity.

3.3. Chaperone activity

Several SurA-like PPIase proteins display chaperone activity, including *Ec*SurA (Bitto and McKay, 2002), *B. pertussis* Par27 (Hodak et al., 2008), *Cj*PEB4 (Kale et al., 2011), and *Bs*PrsA (Jakob et al., 2015). To test whether *Hp*CBF2 has similar activity, we performed an aggregation assay using chemically denatured lysozyme as a model substrate, applying previously with other chaperones (Leroux et al., 1999; Walton and Sousa, 2004). As shown in Fig. 3, increased *Hp*CBF2 concentrations progressively showed decreased absorbance at 320 nm, indicating inhibition of denatured lysozyme aggregation. We notice that, for complete prevention of the lysozyme aggregation it requires twofold excess of *Hp*CBF2. In contrast, negative control BSA proteins had no effect on preventing aggregation of denatured lysozyme (data not shown). Therefore, it is evident that *Hp*CBF2 can impede protein folding to prevent aggregation, which is similar to the chaperone activity of *Cj*PEB4 and other prokaryotic parvulin PPIases. The chaperone activity of *Hp*CBF2 might also help in the binding and transport of client proteins to their target sites.

3.4. Overall structure of HpCBF2-I2CA complex

The crystal structure of the *Hp*CBF2-I2CA complex was determined by SAD method at 2.4 Å resolution (Table 1). The *Hp*CBF2 monomer consists of two domains (Fig. 4A and B): a chaperone domain composed of *N*- and *C*-terminal regions (residues 54–152 and 261–296, respectively), and a PPIase domain (residues 157–254) exhibiting a classical parvulin fold (Yaffe et al., 1997). The chaperone domain of *Hp*CBF2 is comprised of four α-helices (α1, α2, α3 and α8) and two short antiparallel β-strands (β1 and β2) at the *N*-terminal region. The PPIase domain of *Hp*CBF2 contains four antiparallel β-strands (β3, β4, β5 and β6) that are surrounded by four α-helices (α4, α5, α6 and α7). The I2CA molecule was bound by the PPIase domain near to α6, loop β4-α7 and loop β5-β6. The PPIase and chaperone domains are connected by two linkers (residues 148–156 and 255–261) (Fig. 1). The structure of the *Hp*CBF2 PPIase domain closely resembles those of *Cj*PEB4, *Bs*PrsA and *Ec*SurA (Bitto and McKay, 2002; Jakob et al., 2015; Kale et al., 2011) with root mean square deviations (r.m.s. deviation) of 0.4 Å (75 of 98 C_α atoms), 0.6 Å (61 of 89 C_α atoms), and 1.8 Å (77 of 105 C_α atoms), respectively. However, the *Hp*CBF2 chaperone domain alone moderately resembled that of *Cj*PEB4, with a

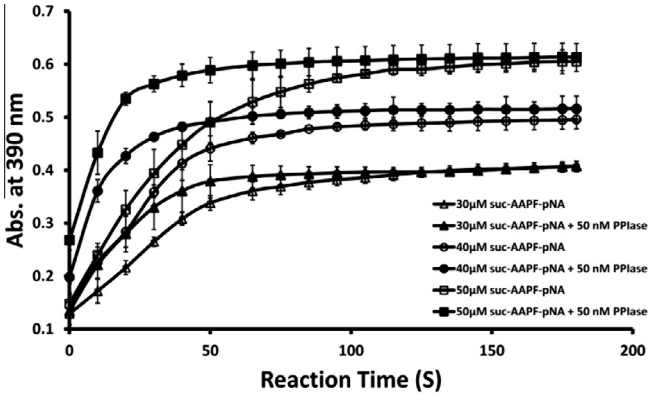

Fig. 2. PPIase activity of *Hp*CBF2. Time-course measurement of cross-peak intensity for chromogenic *p*-nitroaniline α-chymotrypsin measured at 390 nm. Data shown for four replicates of 30 μM, 40 μM and 50 μM of Suc-AAPF-*p*NA coupled with α-chymotrypsin assayed in the presence (closed markers) or absence (open markers) of 50 nM *Hp*CBF2 enzyme.

r.m.s. deviation of 2.0 Å (94 of 143 C_α atoms); the corresponding r.m.s. deviations of the *Hp*CBF2 chaperone domain with those of *Bs*PrsA and *Ec*SurA were 14.1 Å and 5.9 Å, respectively. There is one *Hp*CBF2 homodimer in the asymmetric unit, and each *Hp*CBF2 monomer binds to one I2CA molecule (Fig. 4C). The analytical ultracentrifugation results (AUC) confirm that the molecular weight of *Hp*CBF2 in solution is 60.4 ± 1.6 kDa, which corresponds to a homodimer (Supplemental Fig. S2). This is consistent with our observed derived crystal structure. The two monomers superimposed with a r.m.s. deviation of 1.6 Å for 226 C_α atoms. Interestingly, the chaperone domains of the two monomers interlocked in a "domain-swapped" manner to establish a stable dimer (Fig. 4C and D). Domain-swapping has also been reported for the chaperone domain of *Cj*PEB4 belonging to SurA-like PPIase family (Kale et al., 2011).

3.5. Ligand binding site of HpCBF2

The I2CA-binding site in the PPIase domain of the *Hp*CBF2-I2CA complex was determined by a $F_o - F_c$ omit electron density map (Supplemental Fig. S3). Although the B factors for bound I2CA are higher than the average B factor, it still could trace the clear additional density corresponding to the bound I2CA molecule. In support, high B factors for the bound 6-methyl-1H-indole-2-carboxylic acid (analog of I2CA) (89.8 $Å^2$) than the average *B* factor (45 $Å^2$) was also observed in *Hs*Pin1 (PPIase family protein) (PDB ID: 3KAB) (Potter et al., 2010). Similarly, Pin1 in complex with Ala-Pro substrate show incomplete electron density to the bound ligand (PDB ID: 1PIN) (Ranganathan et al., 1997). The I2CA-binding pocket of *Hp*CBF2 was formed by three β-strands (β3, β5 and β6) acting as a scaffold, surrounded by four α-helices (α4, α5, α6 and α7) (Figs. 4A, B and 5A). The residues involved in I2CA binding were Asp199, Leu211, Met219, Phe223, Phe244 and His247 (Fig. 5A). These residues and their positions are conserved across the SurA-like PPIases studied here. I2CA-binding primarily involves hydrophobic interactions located at the binding pocket. Leu211 (β4), Met219 (loop β4-α7), Phe223 (α7) and His247 (β5) of *Hp*CBF2 were positioned near the indole group of I2CA, whereas Asp199 (loop α5-α6) and Phe244 (loop α7-β5) interacted with the carboxyl terminus of the I2CA molecule. The interactions between *Hp*CBF2 and the I2CA molecule somewhat resemble those of *Hs*PIN1-I2CA analog complex (Potter et al., 2010) due to the position of the small molecule I2CA in *Hp*CBF2-I2CA was not quite similar to that in *Hs*PIN1. The residues of the conserved binding pocket of parvulin-type PPIase including *Hp*CBF2, *Hs*PIN1 (Ranganathan

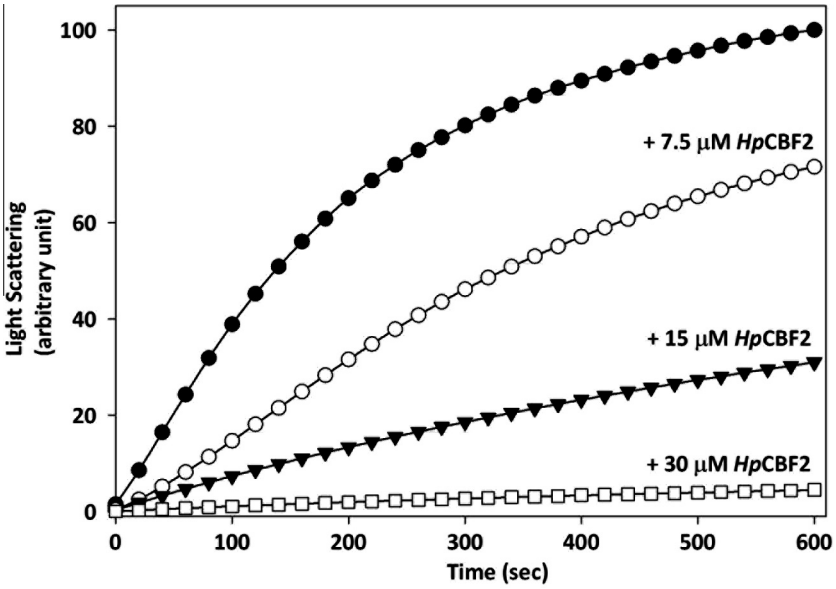

Fig. 3. Chaperone activity of *Hp*CBF2. Aggregation of lysozyme was monitored by light scattering in the presence of *Hp*CBF2. From top to bottom, the curves represent the aggregation behavior of lysozyme at a final concentration of 15 μM in the absence of *Hp*CBF2 (●) and in the presence of *Hp*CBF2 at concentrations of 7.5 (○), 15 (▼), and 30 (□) μM, respectively.

et al., 1997), *Cj*PEB4 (Kale et al., 2011) and *Bs*PrsA (Jakob et al., 2015) are shown in Fig. 5A–D. Among these residues, His161, Leu211, Met219, Phe223 and His247 (numbering as for *Hp*CBF2) are highly conserved in both prokaryotic and human PPIase. However, residue Asp199 is only conserved in prokaryotic PPIase and replaced by cysteine in *Hs*Pin1.

3.6. Structural differences between apo- and I2CA-bound HpCBF2 determined by SAXS

SAXS experiments were conducted to study the conformations of apo- and I2CA-bound *Hp*CBF2 in solution with a pH value of 3.9 which was same as the crystallization condition. The scattering curves of *Hp*CBF2 measured in the presence or absence of I2CA were overlaid and shown in Fig. 6A. Meanwhile, the indirect fourier transformation of these curves yields the corresponding $P(r)$ profiles were calculated using the GNOM program and overlaid as shown in Fig. 6B. The R_g value of both apo- and I2CA-bound *Hp*CBF2 were 34.2 and 33.1 Å, and the maximum dimensions (D_{max}) were 98.0 Å and 97.1 Å, respectively. Minor difference between the scattering curves and the corresponding $P(r)$ profiles of apo- and I2CA-bound *Hp*CBF2 was observed, especially in the high resolution data (Fig. 6A and B). In order to investigate the conformational difference between apo- and I2CA-bound *Hp*CBF2 in solution, the SAXS profile of the *Hp*CBF2-I2CA crystal structure (PDB ID: 5EZ1, in this study) was generated and overlaid with the apo- and ligand-bound *Hp*CBF2 SAXS scattering curves by FoXS program (Fig. 6C and D). Interestingly, the higher Chi (χ) value of 8.2 for fitting with the scattering curve of apo *Hp*CBF2 was observed than that of I2CA-bound *Hp*CBF2 ($\chi = 3.2$). The results suggest that the conformation of the apo- and I2CA-bound *Hp*CBF2 might be different in solution.

Furthermore, although the R_g and D_{max} values were quite similar for both apo- and I2CA-bound *Hp*CBF2, the shape reconstructions from the experimental scattering profiles generated using *ab initio* calculations of them were different (Fig. 6E). The side views of both apo- and I2CA-bound *Hp*CBF2 show central cavity and represent a rhombus-like shape with variation. More distinct differences were observed with respect to the top view, where the apo *Hp*CBF2 resembles W-shape and I2CA-bound *Hp*CBF2 resembles V-shape (Fig. 6E). The surface envelopes of apo- and I2CA-bound *Hp*CBF2 suggest that the conformations of apo- and I2CA-bound states of *Hp*CBF2 in solution might be different.

As the X-ray crystal structure is a snapshot of one conformation that is energetically favorable and the solution scattering is the average of the dynamic motion in solution, structural variation could account for this discrepancy. Since parvulin-type PPIase family proteins are known to be flexible and have conformation variance (Clantin et al., 2010; Riboldi-Tunnicliffe et al., 2001), which supports our lateral hypothesis. Our SAXS data supported that the apo- and I2CA-bound *Hp*CBF2 exhibit different conformations in solution.

3.7. Domain motion in HpCBF2-I2CA complex

To illustrate the dynamic motion and conformational change upon ligand binding in *Hp*CBF2, the crystal structure of the *Hp*CBF2-I2CA complex dimer was compared to the ligand-free *Cj*PEB4 dimer (PDB ID: 3RFW) by superimposition where the chaperone domains were fixed. The r.m.s. deviation was calculated as 3.3 Å for 223 C_α atoms between *Hp*CBF2-I2CA complex and ligand-free *Cj*PEB4 (Fig. 7A). In side view (Fig. 7A), the distance between the C_α of two Phe143 (in the middle of α3) and two Gln279 (in the middle of α8) in each monomer of the *Hp*CBF2-I2CA dimer were 68.1 Å and 47.8 Å, respectively. Whereas, the measured distance between the corresponding residues (Phe120 and Lys254) in *Cj*PEB4, were 63.6 Å and 43.7 Å, respectively. As a consequence, the α3 and α8 helices next to the linker region of the chaperone domain were inclined outward in *Hp*CBF2-I2CA in comparison with that of ligand-free *Cj*PEB4. With respect to the chaperone domains, the included angles between α1 and α2 (Fig. 7A, right panel) of *Hp*CBF2-I2CA complex is 61.3°, which is 10° greater than the ligand-free *Cj*PEB4 (51.3°). The domain swap formed by α1 and α2 of two monomers in the dimer of *Hp*CBF2-I2CA were looser than that of the ligand-free *Cj*PEB4 (Fig. 7A, right panel). The observed conformational alteration of α1, α2, α3 and α8 helices in the chaperone domain might require for the

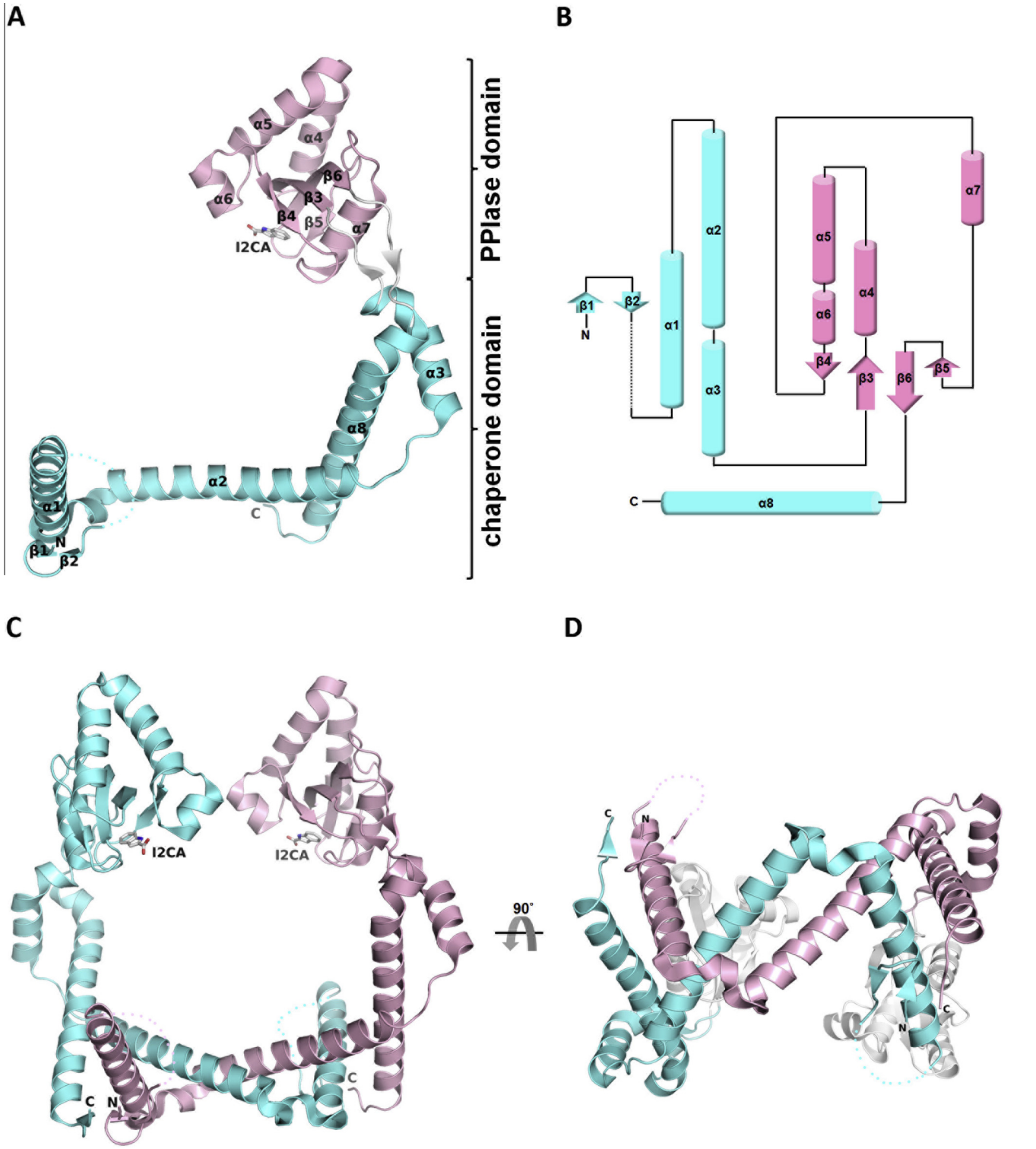

Fig. 4. Overall structure of the *Hp*CBF2-I2CA complex. (A) Ribbon representation of the *Hp*CBF2 monomer. The PPIase and chaperone domains are colored in pink and cyan, respectively. Missing residues (residues 63–74) in the chaperone domain are drawn as a dotted line (cyan). (B) Topology diagram of *Hp*CBF2. The α-helices and β-strands are shown as cylinders and arrows, respectively, with the same color coding as in (A). (C) Ribbon representation of the *Hp*CBF2 homodimer. The two monomers in the asymmetric unit are colored in pink and cyan, respectively. (D) View of the chaperone domain for emphasizing the domain-swapping architecture. The bound ligand I2CA is represented by stick models and CPK coloring. *N*- and *C*-terminals are depicted in both the structure and topology diagrams.

accommodation of unfolded or partially folded peptide or protein to carry out its chaperone function.

With respect to the PPIase domains (Fig. 7A, right panel), the two PPIase domains of the *Hp*CBF2-I2CA complex and ligand-free *Cj*PEB4 positioned in a letter X-like manner. The two PPIase domains in the *Hp*CBF2-I2CA complex are separated by a distance of 22.8 Å (measured between the C_α of two Gln206 residues), whereas the corresponding distance in ligand-free *Cj*PEB4 is 8.2 Å (measured between the C_α of two Gln 182 residues). To further investigate the dynamic motion of *Hp*CBF2-I2CA complex, we mea-

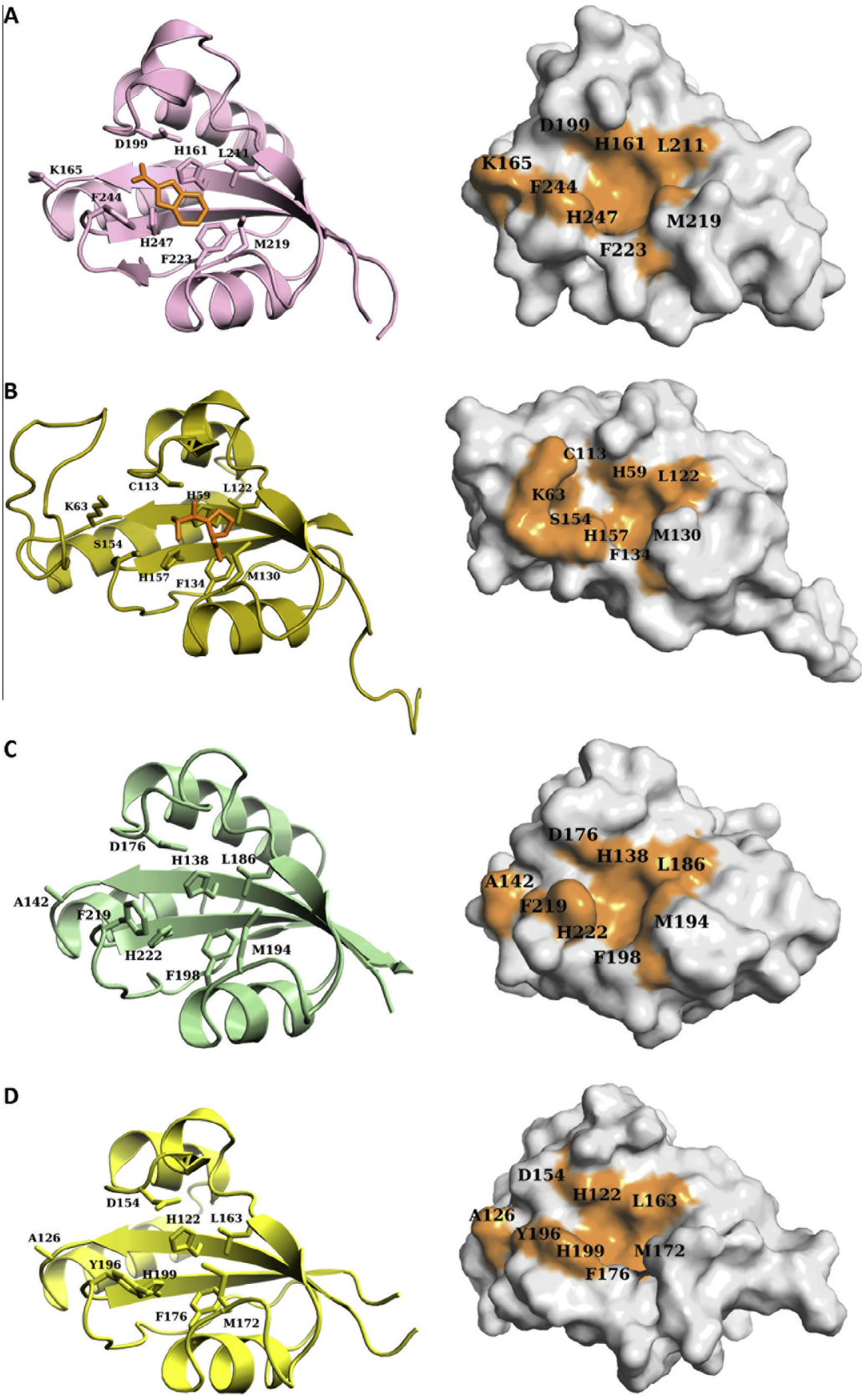

Fig. 5. Ligand-binding pocket of parvulin-family PPIase proteins. Ribbon and surface representation of the PPIase domains from (A) *Hp*CBF2-I2CA complex (*pink*), (B) *Hs*Pin1-AlaPro complex (*sand*, PDB ID: 1PIN), (C) *Cj*PEB4 (*green*, PDB ID: 3RFW) and (D) *Bs*PrsA (*yellow*, PDB ID: 4WO7) in the left and right panels, respectively. The I2CA and Ala-Pro molecules are shown as stick models and are colored orange in (A) and (B). The key residues involved in the binding pocket are labeled and shown as stick models in the ribbon representation, and are colored in orange in the surface representation.

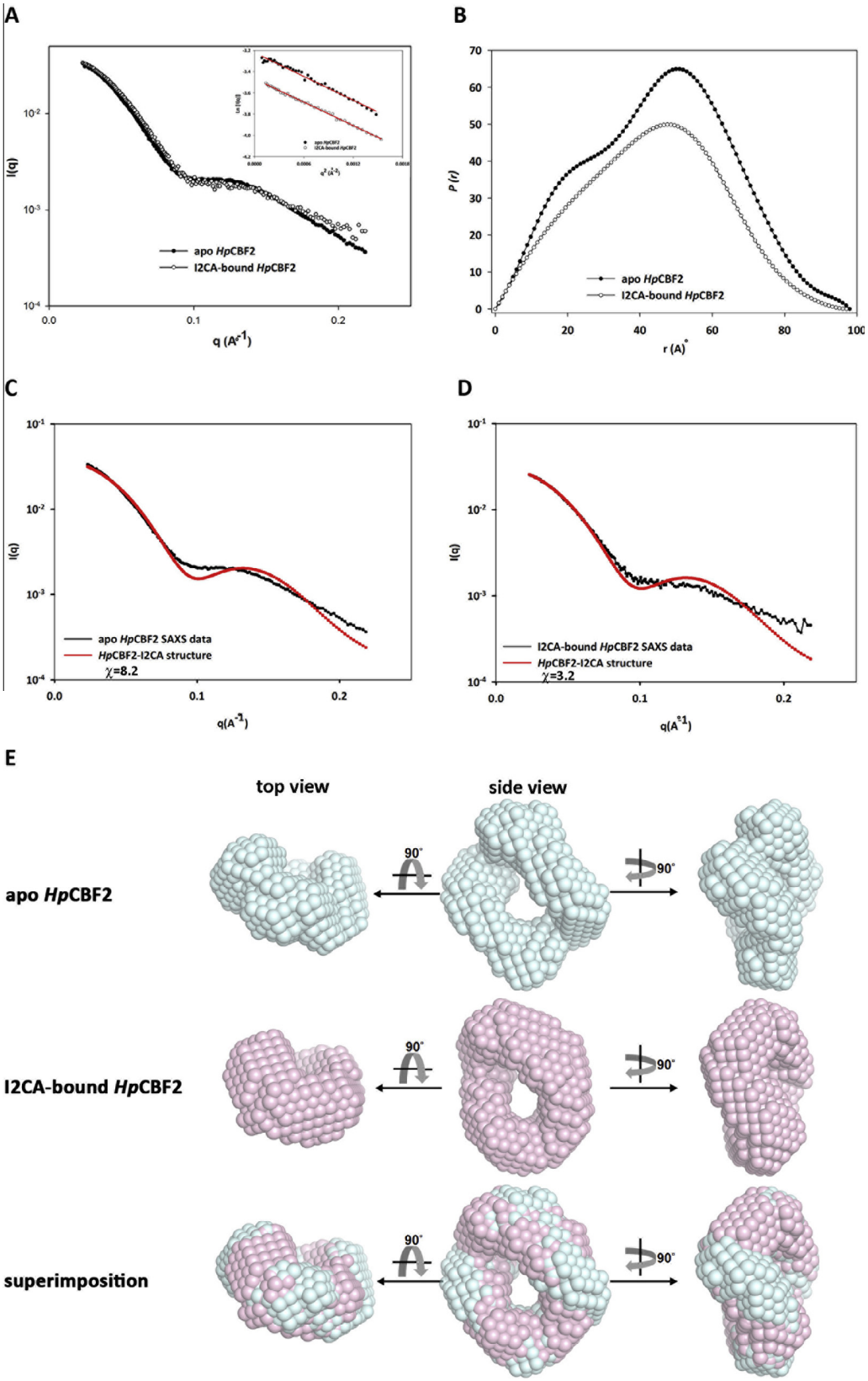

Fig. 6. Small-angle X-ray scattering (SAXS) characterizations of apo- and I2CA-bound *Hp*CBF2 in solution. (A) Overlay of experimental SAXS curves (*black*, open and closed circles for apo- and I2CA-bound *Hp*CBF2) and the inner panel showing the theoretical fitting of the scattering curves at low *Q* (red, open and closed circles for apo- and I2CA-bound *Hp*CBF2). (B) The distance distributions of apo- and I2CA-bound *Hp*CBF2 derived form. The indirect Fourier transformation of SAXS curves showing the corresponding *P* (*r*) profile. (C and D) Overlay of *Hp*CBF2-I2CA structure (PDB ID: 5EZ1, in this study) (red line) with experimental SAXS data (black line) apo *Hp*CBF2 (C) and I2CA-bound *Hp*CBF2 (D). The curves were fitted by FoXS and the respective Chi (χ) values are denoted. (E) Minimized low-resolution envelopes obtained from the 20 independent *ab initio* models of apo- and I2CA-bound *Hp*CBF2 derived from the SAXS data and colored in cyan and pink, respectively. Superimposition and different orientations (rotation along the *x*- or *y*-axis by 90°) of the envelopes are shown for emphasizing the differences among the apo- and I2CA-bound conformations of *Hp*CBF2 in solution.

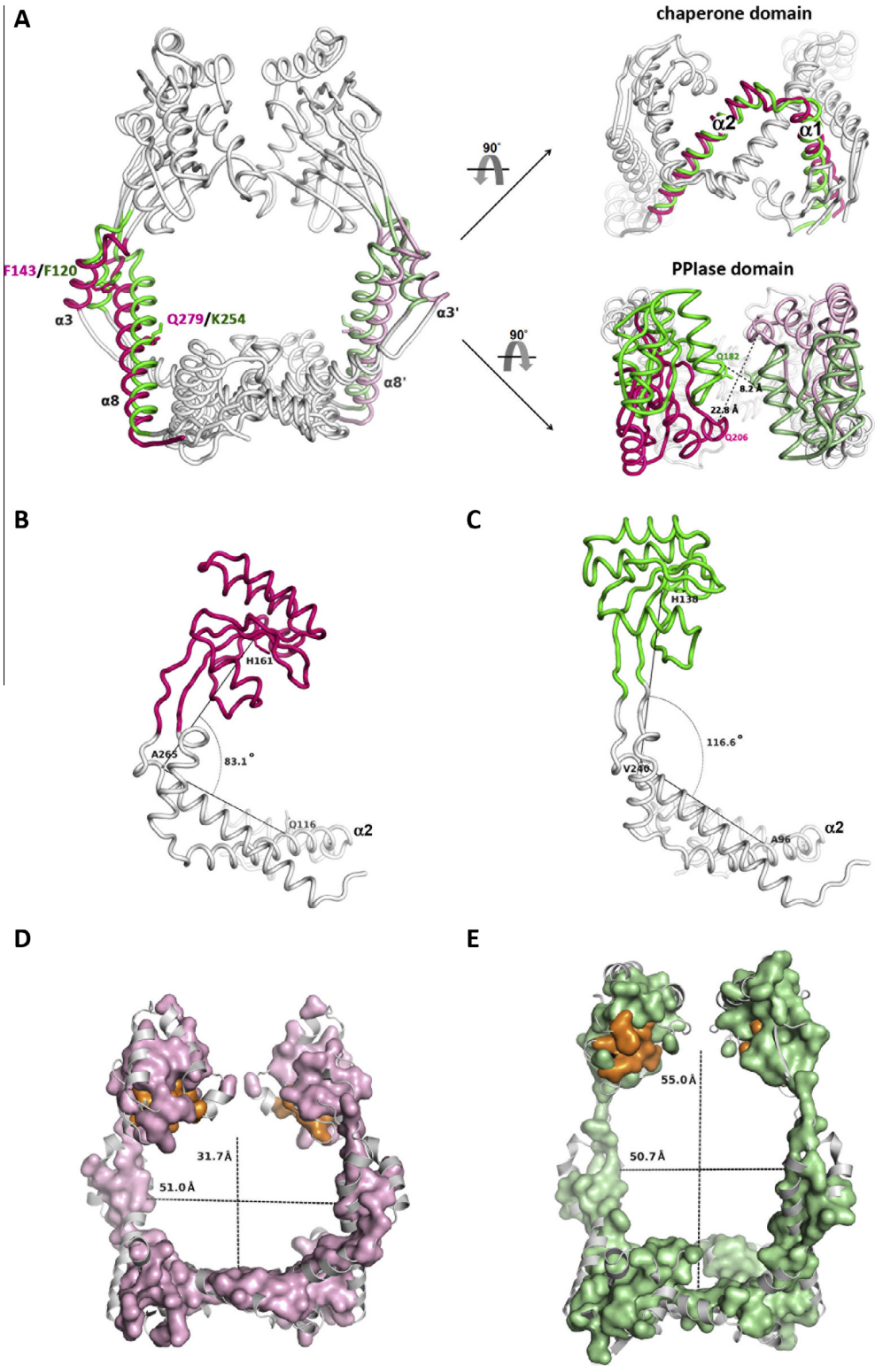

Fig. 7. Structural comparison of *Hp*CBF2-I2CA complex and ligand-free *Cj*PEB4. (A) Superimposition of *Hp*CBF2-I2CA complex and ligand-free *Cj*PEB4 (PDB ID: 3RFW). *N*-terminal chaperone domains were aligned to demonstrate the domain motion in the PPIase domains. The linker connection region (α3 and α8) of the chaperone domains of *Hp*CBF2 and *Cj*PEB4 are colored in magenta and green, respectively. The upper and lower right panel showing the chaperone and PPIase domains of the superimposition. The α1 and α2 are colored as earlier and labeled. In the lower right panel, the PPIase domains of *Hp*CBF2 are colored in magenta and pink, and for *Cj*PEB4, green and slate, respectively. The distance between the two PPIase domains measured from the conserved Gln residues (Gln206 of *Hp*CBF2 and Gln182 of *Cj*PEB4, respectively) are shown. (B and C) Monomer of *Hp*CBF2-I2CA and ligand-free *Cj*PEB4 showing bent angle between PPIase and chaperone domains. The measured angular bent is indicated. The PPIase domains of *Hp*CBF2 and *Cj*PEB4 are colored in magenta and green, respectively and the chaperone domain is colored in gray. (D and E) Surface plot comparison of *Hp*CBF2-I2CA complex and ligand-free *Cj*PEB4 showing the shielding of the active site (orange) and orientation towards the central hydrophobic cavity for *Hp*CBF2. All hydrophobic residues in the chaperone and PPIase domains are shown in surface representation, and colored in pink and green for *Hp*CBF2-I2CA complex and ligand-free *Cj*PEB4, respectively. Non-hydrophobic residues are colored in gray and are shown as ribbons. The dimensions of the central cavity are indicated in a unit of Å. The orientation is same as Fig. 4C. Residues contributing to the active site of the PPIase domain are colored orange.

sured the bent angle between the PPIase and chaperone domains. In *Hp*CBF2-I2CA complex, the bent angle was measured as 83.1° from the three residues, His161 (key residue in the PPIase binding pocket), Ala265 (linker joining the PPIase and chaperone domain), and Gln116 (middle residue of the α2) (Fig. 7B). The bent angle in *Hp*CBF2-I2CA complex is 33.5° smaller than that in the ligand-free *Cj*PEB4 (corresponding residues are His138, Val240, and Ala96) which was measured as 116.6° (Fig. 7C). Furthermore, this dynamic motion result in the shielding of *cis*, *trans* isomerization site in *Hp*CBF2-I2CA complex with the surrounding hydrophobic residues (Fig. 7D). Wherein, the *cis*, *trans* isomerization site is fully exposed in the ligand-free *Cj*PEB4 (Fig. 7E). The measured central cavity of *Hp*CBF2-I2CA complex and ligand-free *Cj*PEB4 were ~31.7 × ~51 Å and ~55 × ~50.7 Å, respectively (Fig. 7D and E). Due to structural alteration in the chaperone domain and the dynamic motion between the PPIase and the chaperone domains, the shape of the central cavity in *Hp*CBF2-I2CA was rearranged to oblate ellipsoid shape, where the ligand-free *Cj*PEB4 exhibits prolate ellipsoid shape. Consequently, the *cis*, *trans* isomerization site of PPIase domains in *Hp*CBF2-I2CA complex bowed toward the chaperone domains. The domain motion in *Hp*CBF2 might be for assisting the isomerization and protecting the bound unfolded or partially folded substrate peptides or proteins from the solvent.

Funding

This work was supported by grants from the Ministry of Science and Technology, Taiwan, Republic of China (MOST 103-2627-M-007-008 and MOST 104-2627-M-007-007 to Y.-J.S., and NSC 101-2311-B-001-023-MY3 to C.-D.H.), Academia Sinica (to C.-D.H.) and National Tsing Hua University, Taiwan, Republic of China (102N2787E1 to Y.-J.S.).

Acknowledgments

We thank Prof. Chun-Cheng Lin at National Tsing Hua University for the preparation of the *cis*-form peptide substrate (Suc-AAPF-*p*NA). We are grateful for access to synchrotron radiation beamline 13B1 and 23A at the National Synchrotron Radiation Research Center (NSRRC) in Taiwan, the Macromolecular X-ray Crystallographic Center of National Tsing Hua University in Taiwan, and beamline BL44XU at SPring-8 in Japan.

Appendix A. Supplementary data

Supplementary data associated with this article can be found, in the online version, at http://dx.doi.org/10.1016/j.jsb.2016.02.002.

References

Adams, P.D., Afonine, P.V., Bunkoczi, G., Chen, V.B., Davis, I.W., Echols, N., Headd, J.J., Hung, L.W., Kapral, G.J., Grosse-Kunstleve, R.W., McCoy, A.J., Moriarty, N.W., Oeffner, R., Read, R.J., Richardson, D.C., Richardson, J.S., Terwilliger, T.C., Zwart, P.H., 2010. PHENIX: a comprehensive Python-based system for macromolecular structure solution. Acta Crystallogr. D Biol. Crystallogr. 66, 213–221.

Amedei, A., Munari, F., Bella, C.D., Niccolai, E., Benagiano, M., Bencini, L., Cianchi, F., Farsi, M., Emmi, G., Zanotti, G., de Bernard, M., Kundu, M., D'Elios, M.M., 2014. *Helicobacter pylori* secreted peptidyl prolyl cis, trans-isomerase drives Th17 inflammation in gastric adenocarcinoma. Intern. Emerg. Med. 9, 303–309.

Atanassov, C., Pezennec, L., d'Alayer, J., Grollier, G., Picard, B., Fauchere, J.L., 2002. Novel antigens of *Helicobacter pylori* correspond to ulcer-related antibody pattern of sera from infected patients. J. Clin. Microbiol. 40, 547–552.

Basak, C., Pathak, S.K., Bhattacharyya, A., Pathak, S., Basu, J., Kundu, M., 2005. The secreted peptidyl prolyl cis, trans-isomerase HP0175 of *Helicobacter pylori* induces apoptosis of gastric epithelial cells in a TLR4- and apoptosis signal-regulating kinase 1-dependent manner. J. Immunol. 174, 5672–5680.

Basu, S., Pathak, S.K., Chatterjee, G., Pathak, S., Basu, J., Kundu, M., 2008. *Helicobacter pylori* protein HP0175 transactivates epidermal growth factor receptor through TLR4 in gastric epithelial cells. J. Biol. Chem. 283, 32369–32376.

Bitto, E., McKay, D.B., 2002. Crystallographic structure of SurA, a molecular chaperone that facilitates folding of outer membrane porins. Structure 10, 1489–1498.

Bose, S., Freedman, R.B., 1994. Peptidyl prolyl cis–trans-isomerase activity associated with the lumen of the endoplasmic reticulum. Biochem. J. 300 (Pt. 3), 865–870.

Clantin, B., Leyrat, C., Wohlkonig, A., Hodak, H., Ribeiro Ede Jr., A., Martinez, N., Baud, C., Smet-Nocca, C., Villeret, V., Jacob-Dubuisson, F., Jamin, M., 2010. Structure and plasticity of the peptidyl-prolyl isomerase Par27 of *Bordetella pertussis* revealed by X-ray diffraction and small-angle X-ray scattering. J. Struct. Biol. 169, 253–265.

Davis, I.W., Leaver-Fay, A., Chen, V.B., Block, J.N., Kapral, G.J., Wang, X., Murray, L.W., Arendall 3rd, W.B., Snoeyink, J., Richardson, J.S., Richardson, D.C., 2007. MolProbity: all-atom contacts and structure validation for proteins and nucleic acids. Nucleic Acids Res. 35, W375–W383.

Delano, W.L., 2010. The PyMOL Molecular Graphics System Version 1.3r1. Schrödinger, LLC, New York.

Emsley, P., Cowtan, K., 2004. Coot: model-building tools for molecular graphics. Acta Crystallogr. D Biol. Crystallogr. 60, 2126–2132.

Girardini, J.E., Napoli, M., Piazza, S., Rustighi, A., Marotta, C., Radaelli, E., Capaci, V., Jordan, L., Quinlan, P., Thompson, A., Mano, M., Rosato, A., Crook, T., Scanziani, E., Means, A.R., Lozano, G., Schneider, C., Del Sal, G., 2011. A Pin1/mutant p53 axis promotes aggressiveness in breast cancer. Cancer Cell 20, 79–91.

Giuseppe, P.O., Von Atzingen, M., Nascimento, A.L., Zanchin, N.I., Guimaraes, B.G., 2011. The crystal structure of the leptospiral hypothetical protein LIC12922 reveals homology with the periplasmic chaperone SurA. J. Struct. Biol. 173, 312–322.

Gong, Y.H., Chen, M., Xu, Y., Dong, N., Sang, Z., Liu, J., Yuan, Y., 2011. Subtractive hybridization analysis of gastric diseases-associated *Helicobacter pylori* identifies peptidyl-prolyl isomerase as a potential marker for gastric cancer. FEMS Microbiol. Lett. 320, 103–109.

Gouet, P., Courcelle, E., Stuart, D.I., Metoz, F., 1999. ESPript: analysis of multiple sequence alignments in PostScript. Bioinformatics 15, 305–308.

Halder, P., Datta, C., Kumar, R., Sharma, A.K., Basu, J., Kundu, M., 2015. The secreted antigen, HP0175, of *Helicobacter pylori* links the unfolded protein response (UPR) to autophagy in gastric epithelial cells. Cell. Microbiol. 17, 714–729.

Hennig, L., Christner, C., Kipping, M., Schelbert, B., Rucknagel, K.P., Grabley, S., Kullertz, G., Fischer, G., 1998. Selective inactivation of parvulin-like peptidyl-prolyl cis/trans isomerases by juglone. Biochemistry 37, 5953–5960.

Hodak, H., Wohlkonig, A., Smet-Nocca, C., Drobecq, H., Wieruszeski, J.M., Senechal, M., Landrieu, I., Locht, C., Jamin, M., Jacob-Dubuisson, F., 2008. The peptidyl-prolyl isomerase and chaperone Par27 of *Bordetella pertussis* as the prototype for a new group of parvulins. J. Mol. Biol. 376, 414–426.

Ikolo, F., Zhang, M., Harrington, D.J., Robinson, C., Waller, A.S., Sutcliffe, I.C., Black, G. W., 2015. Characterisation of SEQ0694 (PrsA/PrtM) of *Streptococcus equi* as a functional peptidyl-prolyl isomerase affecting multiple secreted protein substrates. Mol. BioSyst. 11, 3279–3286.

Jakob, R.P., Koch, J.R., Burmann, B.M., Schmidpeter, P.A., Hunkeler, M., Hiller, S., Schmid, F.X., Maier, T., 2015. Dimeric structure of the bacterial extracellular foldase PrsA. J. Biol. Chem. 290, 3278–3292.

Kale, A., Phansopa, C., Suwannachart, C., Craven, C.J., Rafferty, J., Kelly, D.J., 2011. The virulence factor PEB4 and the periplasmic protein Cj1289 are two structurally related SurA-like chaperones in the human pathogen *Campylobacter jejuni*. J. Biol. Chem.

Konarev, P.V., Volkov, V.V., Sokolova, A.V., Koch, M.H.J., Svergun, D.I., 2003. PRIMUS: a windows PC-based system for small-angle scattering data analysis. J. Appl. Crystallogr. 36, 1277–1282.

Kozin, M.B., Svergun, D.I., 2001. Automated matching of high- and low-resolution structural models. J. Appl. Crystallogr. 34, 33–41.

Kullertz, G., Luthe, S., Fischer, G., 1998. Semiautomated microtiter plate assay for monitoring peptidylprolyl cis/trans isomerase activity in normal and pathological human sera. Clin. Chem. 44, 502–508.

Lang, K., Schmid, F.X., Fischer, G., 1987. Catalysis of protein folding by prolyl isomerase. Nature 329, 268–270.

Lazar, S.W., Kolter, R., 1996. SurA assists the folding of *Escherichia coli* outer membrane proteins. J. Bacteriol. 178, 1770–1773.

Lee, T.H., Pastorino, L., Lu, K.P., 2011. Peptidyl-prolyl cis–trans isomerase Pin1 in ageing, cancer and Alzheimer disease. Expert Rev. Mol. Med. 13.

Leroux, M.R., Fandrich, M., Klunker, D., Siegers, K., Lupas, A.N., Brown, J.R., Schiebel, E., Dobson, C.M., Hartl, F.U., 1999. MtGimC, a novel archaeal chaperone related to the eukaryotic chaperonin cofactor GimC/prefoldin. EMBO J. 18, 6730–6743.

Liou, Y.C., Zhou, X.Z., Lu, K.P., 2011. Prolyl isomerase Pin1 as a molecular switch to determine the fate of phosphoproteins. Trends Biochem. Sci. 36, 501–514.

Lu, K.P., Zhou, X.Z., 2007. The prolyl isomerase PIN1: a pivotal new twist in phosphorylation signalling and disease. Nat. Rev. Mol. Cell Biol. 8, 904–916.

Lu, K.P., Finn, G., Lee, T.H., Nicholson, L.K., 2007. Prolyl cis–trans isomerization as a molecular timer. Nat. Chem. Biol. 3, 619–629.

Marchler-Bauer, A., Derbyshire, M.K., Gonzales, N.R., Lu, S., Chitsaz, F., Geer, L.Y., Geer, R.C., He, J., Gwadz, M., Hurwitz, D.I., Lanczycki, C.J., Lu, F., Marchler, G.H., Song, J.S., Thanki, N., Wang, Z., Yamashita, R.A., Zhang, D., Zheng, C., Bryant, S.H., 2015. CDD: NCBI's conserved domain database. Nucleic Acids Res. 43, D222–D226.

Matthews, B.W., 1968. Solvent content of protein crystals. J. Mol. Biol. 33, 491–497.

McAtee, C.P., Lim, M.Y., Fung, K., Velligan, M., Fry, K., Chow, T.P., Berg, D.E., 1998. Characterization of a *Helicobacter pylori* vaccine candidate by proteome techniques. J. Chromatogr. B Biomed. Sci. Appl. 714, 325–333.

Motohashi, K., Koyama, F., Nakanishi, Y., Ueoka-Nakanishi, H., Hisabori, T., 2003. Chloroplast cyclophilin is a target protein of thioredoxin. J. Biol. Chem. 278, 31848–31852.
Otwinowski, Z., Minor, W., 1997. Processing of X-ray diffraction data collected in oscillation mode. Method Enzymol. 276, 307–326.
Pathak, S.K., Basu, S., Bhattacharyya, A., Pathak, S., Banerjee, A., Basu, J., Kundu, M., 2006. TLR4-dependent NF-kappaB activation and mitogen- and stress-activated protein kinase 1-triggered phosphorylation events are central to *Helicobacter pylori peptidyl* prolyl cis-, trans-isomerase (HP0175)-mediated induction of IL-6 release from macrophages. J. Immunol. 177, 7950–7958.
Petoukhov, M.V., Konarev, P.V., Kikhney, A.G., Svergun, D.I., 2007. ATSAS 2.1 – towards automated and web-supported small-angle scattering data analysis. J. Appl. Crystallogr. 40, S223–S228.
Pierson, N.A., Chen, L.X., Russell, D.H., Clemmer, D.E., 2013. Cis–trans isomerizations of proline residues are key to bradykinin conformations. J. Am. Chem. Soc. 135, 3186–3192.
Potter, A.J., Ray, S., Gueritz, L., Nunns, C.L., Bryant, C.J., Scrace, S.F., Matassova, N., Baker, L., Dokurno, P., Robinson, D.A., Surgenor, A.E., Davis, B., Murray, J.B., Richardson, C.M., Moore, J.D., 2010. Structure-guided design of α-amino acid-derived Pin1 inhibitors. Bioorg. Med. Chem. Lett. 20, 586–590.
Rahfeld, J.U., Rucknagel, K.P., Schelbert, B., Ludwig, B., Hacker, J., Mann, K., Fischer, G., 1994. Confirmation of the existence of a third family among peptidyl-prolyl cis/trans isomerases. Amino acid sequence and recombinant production of parvulin. FEBS Lett. 352, 180–184.
Ranganathan, R., Lu, K.P., Hunter, T., Noel, J.P., 1997. Structural and functional analysis of the mitotic rotamase Pin1 suggests substrate recognition is phosphorylation dependent. Cell 89, 875–886.
Riboldi-Tunnicliffe, A., Konig, B., Jessen, S., Weiss, M.S., Rahfeld, J., Hacker, J., Fischer, G., Hilgenfeld, R., 2001. Crystal structure of Mip, a prolylisomerase from *Legionella pneumophila*. Nat. Struct. Biol. 8, 779–783.
Schneidman-Duhovny, D., Hammel, M., Sali, A., 2010. FoXS: a web server for rapid computation and fitting of SAXS profiles. Nucleic Acids Res. 38, W540–W544.
Schneidman-Duhovny, D., Hammel, M., Tainer, J.A., Sali, A., 2013. Accurate SAXS profile computation and its assessment by contrast variation experiments. Biophys. J . 105, 962–974.
Siekierka, J.J., Hung, S.H., Poe, M., Lin, C.S., Sigal, N.H., 1989. A cytosolic binding protein for the immunosuppressant FK506 has peptidyl-prolyl isomerase activity but is distinct from cyclophilin. Nature 341, 755–757.
Svergun, D.I., 1992. Determination of the regularization parameter in indirect-transform methods using perceptual criteria. J. Appl. Crystallogr. 25, 495–503.
Svergun, D.I., 1999. Restoring low resolution structure of biological macromolecules from solution scattering using simulated annealing. Biophys. J . 76, 2879–2886.
Tatara, Y., Lin, Y.C., Bamba, Y., Mori, T., Uchida, T., 2009. Dipentamethylene thiuram monosulfide is a novel inhibitor of Pin1. Biochem. Biophys. Res. Commun. 384, 394–398.
Terwilliger, T.C., Adams, P.D., Read, R.J., McCoy, A.J., Moriarty, N.W., Grosse-Kunstleve, R.W., Afonine, P.V., Zwart, P.H., Hung, L.W., 2009. Decision-making in structure solution using Bayesian estimates of map quality: the PHENIX AutoSol wizard. Acta Crystallogr. D Biol. Crystallogr. 65, 582–601.
Volkov, V.V., Svergun, D.I., 2003. Uniqueness of ab initio shape determination in small-angle scattering. J. Appl. Crystallogr. 36, 860–864.
Walton, T.A., Sousa, M.C., 2004. Crystal structure of Skp, a prefoldin-like chaperone that protects soluble and membrane proteins from aggregation. Mol. Cell 15, 367–374.
Yaffe, M.B., Schutkowski, M., Shen, M., Zhou, X.Z., Stukenberg, P.T., Rahfeld, J.U., Xu, J., Kuang, J., Kirschner, M.W., Fischer, G., Cantley, L.C., Lu, K.P., 1997. Sequence-specific and phosphorylation-dependent proline isomerization: a potential mitotic regulatory mechanism. Science 278, 1957–1960.